Contents lists available at ScienceDirect

Digital Chinese Medicine

journal homepage: http://www.keaipublishing.com/dcmed

Research on resting spontaneous brain activity and functional connectivity of acupuncture at uterine acupoints

YUAN Hang[a, b], YU Xiaohua[c], LI Xiang[a, b], QIN Sijun[a, b], LIANG Guixiang[a, b], BAI Tianyu[d], WEI Benzheng[a, b*]

a. Qingdao Academy of Chinese Medical Sciences, Shandong University of Traditional Chinese Medicine, Qingdao, Shandong 266112, China
b. Center for Medical Artificial Intelligence, Shandong University of Traditional Chinese Medicine, Qingdao, Shandong 266112, China
c. School of Acupuncture-Moxibustion and Tuina, Shandong University of Traditional Chinese Medicine, Jinan, Shandong 250355, China
d. Department of Acupuncture-Moxibustion and Tuina, Shandong Provincial Third Hospital, Jinan, Shandong 250031, China

A R T I C L E   I N F O

Article history
Received 09 December 2021
Accepted 21 January 2022
Available online 25 March 2022

Keywords
Uterine acupoints
Acupuncture
Functional magnetic resonance imaging
Local spontaneous brain activity analysis
Resting state
Functional connectivity

A B S T R A C T

Objective The resting-state functional magnetic resonance imaging (rs-fMRI) method was used to observe brain activity and its functional connection upon electroacupuncture stimulation at bilateral uterine acupoints (EX-CA1), as well as to investigate the mechanism of acupuncture in the treatment of gynecological diseases.

Methods Twenty-two healthy female subjects were stimulated by electroacupuncture at bilateral uterine acupoints; rs-fMRI data of the brain were acquired and standardized. Degree centrality (DC), amplitude of low-frequency fluctuation (ALFF), and regional homogeneity (ReHo) were used to analyze local spontaneous brain activity via acupuncture. An independent component analysis was used to evaluate the functional connectivity of the resting brain networks after acupuncture.

Results Analytical results showed that the neural activity intensity of the precuneus lobe, orbitofrontal cortex, lingual gyrus, amygdala, and posterior central gyrus decreased after acupuncture (voxel $P < 0.001$, cluster $P < 0.05$). Functional connectivity analysis revealed weakened auditory and right frontal-parietal networks (voxel $P < 0.001$, cluster $P < 0.05$), enhanced visual network (voxel $P < 0.001$, cluster $P < 0.05$), and synergistic auditory network and hypothalamic-pituitary system.

Conclusion Significant differences in neural activity and functional connectivity in specific brain regions were observed after acupuncture intervention at uterine acupoints; the hypothalamic-pituitary system also showed various active states in different brain regions. It is speculated that the effective mechanism of acupuncture at uterine acupoints is related to the regulation of reproductive hormones, emotional changes, and somatic sensations. Therefore, the methods used in this study could clarify the neural mechanism of uterine-point acupuncture in the treatment of gynecological diseases and may serve as a reference for other studies pertaining to acupuncture.

1 Introduction

Uterine acupoints (EX-CA1) are the main acupoints of the uterus, which regulate menstruation and promote Qi [1]. It is responsible for irregular menstruation, uterine prolapse, dysmenorrhea, and other symptoms [2]. However, regardless of its significance in treating gynecological diseases, the mechanism of acupuncture at uterine acupoints

*Corresponding author: WEI Benzheng, Professor, E-mail: wbz99@sina.com.

Peer review under the responsibility of Hunan University of Chinese Medicine.

DOI: 10.1016/j.dcmed.2022.03.006
Citation: YUAN H, YU XH, LI X, et al. Research on resting spontaneous brain activity and functional connection of acupuncture at uterine acupoints. Digital Chinese Medicine, 2022, 5(1): 59–67.

remains unclear and requires further investigation [3].

Resting-state functional magnetic resonance imaging (rs-fMRI) can locate various functional regions of the brain by measuring changes in regional perfusion, which is of great significance in clinical neurology research. Combining acupuncture and functional brain activities could objectively indicate the activation or inhibition state of acupuncture in specific areas, providing a powerful tool for studying the mechanism of acupuncture at the uterine acupoints [4].

After acupuncture intervention, local spontaneous brain activity could be determined via analytical methods such as degree centrality (DC), regional homogeneity (ReHo), and amplitude of low-frequency fluctuation (ALFF). DC is commonly used to measure the importance of one voxel as a network node in the brain region [5]. ReHo describes the time-series similarity between voxels and their adjacent counterparts using the Kendall harmony coefficient [6]. ALFF reveals the blood oxygen level-dependent (BOLD) signal intensity of regional spontaneous activity in the resting state, which is reflected among regional brain interactions to produce its own rhythmic pattern [7].

Functional connectivity indicates interactive strength across brain regions; brain regions with high functional connection correlations could constitute the resting-state network (RSN). Independent component analysis (ICA), a data-driven analysis method, can automatically separate meaningful RSNs from fMRI data without any prior knowledge. This feature enables ICA to accurately describe the functional connections of the brain after uterine-point acupuncture.

Based on rs-fMRI, we evaluated the brain activity and its functional connection with uterine acupoint by using acupuncture; this study entails two perspectives. Specifically, three analytical methods (DC, ReHo, and ALFF) were used to measure spontaneous brain activity, and the ICA method was used to explore the effect of uterine-stimulating electroacupuncture on functional brain connectivity. This study provides an imaging basis for exploring the mechanism of acupuncture at uterine acupoints and research ideas or analytical methods for related studies.

2 Data acquisition and preprocessing

2.1 Data acquisition

2.1.1 Inclusion criteria Twenty-two healthy female volunteers were recruited for this study. The inclusion criteria were as follows: (i) age between 20 and 30 years; (ii) right-handedness; (iii) no history of mental or nervous system diseases; (iv) normal menstruation; (v) no history of drug use or acupuncture treatment within two weeks before data collection; and (vi) informed consent.

2.1.2 Exclusion criteria The exclusion criteria were as follows: (i) patients with contraindications to MRI scanning such as metallic products, cardiac pacemakers, and non-removable metal dentures, with claustrophobia, or those who could not undergo MRI scanning for other reasons; (ii) pregnant or lactating women; (iii) history of alcohol or drug abuse; and (iv) contraindications to acupuncture and moxibustion.

2.1.3 Ethical and clinical registration This study was approved by the Ethics Committee of the Third Hospital of Shandong Province (Ethics No. KYLL-2021038) and was registered at www.chictr.org.cn (Registered No. ChiCTR2100047812). All volunteers were informed of the entire experimental process and have provided written informed consent before data collection.

2.2 Electroacupuncture stimulation method

The subjects laid flat on the treatment bed with an exposed lower abdomen. We selected 0.40 mm × 25 mm, Huatuo-branded, disposable acupuncture needles; these were directly inserted into a sterilized acupoint for approximately 25 mm. After needling Qi, the electroacupuncture instrument was connected to both uterine acupoints, selecting a continuous wave with a frequency of 1 Hz and maintaining the needle for 20 min. Twenty-two subjects were operated on by the same acupuncturist; functional magnetic resonance scanning was performed after acupuncture intervention.

2.3 fMRI scanning program and parameters

The image data of the subjects before and after acupuncture were collected using a Philips Ingenia 3.0 T magnetic resonance scanner. Before scanning, the head of all subjects was fixed with anti-noise earplugs and sponges. During the examination, the participants were required to lie flat on the examination table, keep their heads still, and avoid thinking; fMRI data were obtained using an echo plane imaging sequence located by the anterior commissure-posterior commissure (AC-PC) line. The parameter settings were as follows: TR = 2 000 ms, TE = 30 ms, rotation angle = 90°, matrix = 64 × 64, FOV = 220 mm × 220 mm, number of layers = 20, layer thickness = 6 mm, thickness interval = 1 mm. As a result, a total of 180 time points were collected from the brain region.

2.4 fMRI image data preprocessing

To reduce the error caused by data acquisition and ensure the credibility and sensitivity of subsequent analyses, the Data Processing & Analysis for Brain Imaging (DPABI) software based on the MATLAB 2018b platform was used for data processing [8]. The preprocessing steps included: (i) removing the data of the first 10 scanning time points; (ii) time horizon correction; (iii) head movement correction (excluding subjects with average head movement amplitude > 1 mm or rotation parameter > 1° in axes X, Y, and Z); (iv) the EPI template was used for spatial standardization and resampling was 3 mm × 3 mm × 3 mm resolution.

2.5 Comparison of average head movement

A paired sample t test was used to compare the average head movement parameters between the two groups before and after acupuncture. Statistical significance was set at $P < 0.01$; no significant difference was found between the groups ($P > 0.05$).

3 Research method of brain activity and functional connectivity

To explore the mechanism of EX-CA1-stimulating electroacupuncture, we designed an analytical method that could evaluate brain activity and functional connectivity after acupuncture by utilizing brain fMRI data (Figure 1). It is worth noting that DC, ReHo, and ALFF were calculated using DPABI software; ICA was performed using the Group ICA of fMRI Toolbox (GIFT, https://trendscenter.org/software/gift/).

3.1 Analysis of local spontaneous brain activity

3.1.1 DC calculation Before calculating DC, we preprocessed the fMRI data as follows: (i) remove linear drift; (ii) remove covariates such as Friston 24 head movement parameters, cerebrospinal fluid, brain white matter, and whole-brain mean signal; and (iii) use a band-pass filter of 0.01 – 0.1 Hz to eliminate the impact of noise caused by physiologic activities such as breathing and heartbeat on the research results.

As shown in Formulas (1) and (2), the correlation coefficient r_{ij} for the two-voxel time series is calculated using the Pearson correlation coefficient. Subsequently, the DC value of the voxel can be obtained by accumulating the correlation coefficients of $r \gg r_{th}$.

$$r_{ij} = \frac{\sum_{i=1}^{n} \left(x_i - \bar{X}\right)\left(y_i - \bar{X}\right)}{\sum_{i=1}^{n} \sum_{i=1}^{n} \left(x_i - \bar{Y}\right)^2 \left(y_i - \bar{Y}\right)^2} \tag{1}$$

$$a_{ij} = \begin{cases} 0, & r_{ij} < r_{th} \\ r_{ij}, & r_{ij} \geqslant r_{th} \end{cases} \tag{2}$$

Where x_i and y_i represent the time series of two voxels respectively; $\bar{X}$ and $\bar{Y}$ represent voxel-wise means; r_{ij} is the correlation of the time series between voxel x_i and voxel y_i; and r_{th} indicates the threshold; $r_{th} = 0.25$ was selected to remove the correlation caused by physiological noise; and a_{ij} indicates the value of the correlation coefficient after comparison with the threshold.

A standardized method was necessary to process the DC values to ignore the individual differences between the subjects. Specifically, the DC value of a certain voxel minus the average DC value of the whole brain voxel was divided by the standardization deviation of the whole brain DC. The calculation process is expressed as follows.

$$zdc_i = \frac{dc_i - mean(dc)}{std(dc)}, i \in n \tag{3}$$

Where dc and i represent the whole-brain DC value and the voxels in the brain, respectively.

The standardized zdc must be smooth to improve the signal-to-noise ratio and the errors caused by spatial standardization; the size of the smoothing core is 6 mm.

3.1.2 ReHo calculation The preprocessed fMRI data must be denoised in accordance with the DC calculation steps to calculate the ReHo value. ReHo is reflected by the Kendall harmony coefficient, which represents the consistency trend of one or more voxel time courses; the higher the consistency, the closer the Kendall harmony coefficient. Moreover, the stronger the synchronization of

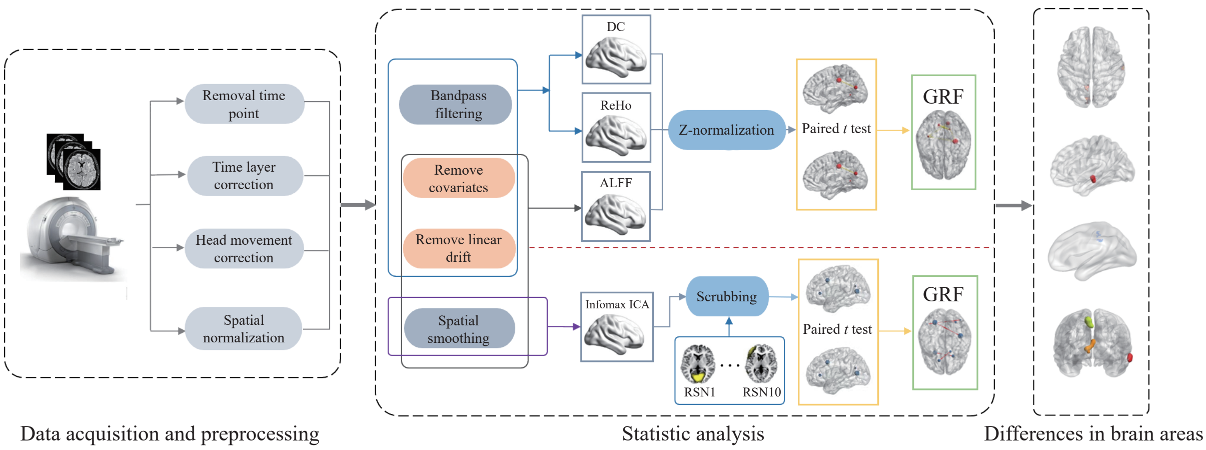

Figure 1 Flow chart of the research methods of the study

the time series in local brain regions, the stronger the functional connectivity between adjacent voxels. The calculation method is as follows.

$$W = \frac{\sum_{i=1}^{n} (R_i)^2 - n(\bar{R})^2}{\frac{1}{12}K^2(n^3 - n)} \quad (4)$$

Where W represents the Kendall harmony coefficient; n is the number of time points; R_i $(i = 1, 2, 3, \ldots, n)$ is the rank sum of the signal values of all adjacent voxel points at the i^{th} time point; $\bar{R}$ is the average of R_i; and K is the total number of elements and all adjacent voxels.

ReHo needs to be standardized and smoothed before statistical analysis. The standardization process is shown in Formula (3); the size of the smoothing kernel was 6 mm.

3.1.3 ALFF calculation Before calculating the ALFF, it is also necessary to further process the preprocessed fMRI data. In particular, in contrast to the aforementioned methods of DC and ReHo, the processing flow of ALFF is as follows: (i) remove linear drift; (ii) remove covariates such as Friston24 head movement parameters, cerebrospinal fluid, brain white matter, and whole-brain mean signal; and (iii) perform spatial smoothing using a 6 mm smoothing kernel.

The processed time series $x(t)$ of each voxel was obtained by fast Fourier transform; the power spectrum was squared, and the sum of the corresponding amplitudes of all frequencies within 0.01 – 0.1 Hz was calculated as ALFF. The calculation formula is as follows.

$$x(t) = \sum_{k=1}^{n} [a_k \cos(2\pi f_k t) + b_k \sin(2\pi f_k t)] \quad (5)$$

$$ALFF = \sum_{K: f_k \in [0.01, 0.1]} \sqrt{\frac{a_k^2(f) + b_k^2(f)}{N}} \quad (6)$$

Where $f_k t$ represents frequency; t represents time; $x(t)$ represents power spectrum; and a_k and b_k represent amplitudes. Whole-brain ALFF results were obtained using voxel-by-voxel calculation. Before statistical analysis, the ALFF needs to be standardized. The standardization process is shown in Formula (3).

3.2 Functional connectivity analysis

The Infomax ICA method [9] was used for spatially smoothing the preprocessed fMRI data; the spatial smoothing kernel was 6 mm. The fMRI data of each subject were decomposed into 43 independent spatial components; correlation analysis was conducted between the spatial components decomposed before and after acupuncture and the selected reference template. Ultimately, a paired t test and GRF correction were performed to compare the functional connectivity differences before and after acupuncture.

The final entropy transformation of the Infomax ICA function can be expressed as follows.

$$u = Wx \quad (7)$$

$$\begin{aligned} H(y) &= H\left[g_1\left(w_1^T x\right), \ldots, g_n\left(w_n^T x\right)\right] \\ &= H(x) + \sum_i E\left\{\log g_i^{'}\left(w_i^T x\right)\right\} = \log|detW| \end{aligned} \quad (8)$$

Where $H(y)$ represents the marginal entropy of the output; $g_i\left(w_n^T x\right)$ $(i = 1, 2, 3, \ldots, n)$ represents the output of a reversible monotone nonlinear function; x represents the input signal; W represents the iterative matrix; $u = Wx$ is deduced based on the feedforward neural network theory and represents the maximal equivalence of the non-Gaussian property of u and the non-Gaussian property of y.

In the above calculation process, to better compare the functional connectivity of the brain after acupuncture intervention and to aim at the data of healthy subjects collected in the study, we selected 10 RSNs isolated by SMITH et al. [10] as an a priori template. Furthermore, we included the visual (IN1, IN2, and IN3), default mode (IN4), cerebellum (IN5), sensorimotor (IN6), auditory (IN7), executive control (IN8), and left and right frontal-parietal networks (IN9 and IN10) in this study. A schematic of the 10 RSNs selected for this study is shown in Figure 2.

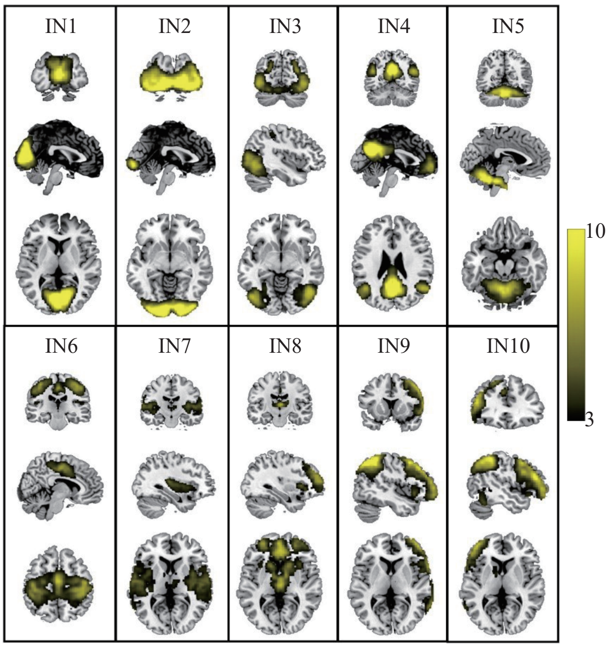

Figure 2 Schematic diagrams of 10 RSNs selected in the research

4 Statistical analysis and results

4.1 DC analysis

The experimental results obtained using the DC method are shown in Table 1; the visualization results of the wedge leaf and lingual gyrus are shown in Figure 3. After

Table 1 Statistical analysis of DC difference brain area after acupuncture intervention

Brain region	Hemisphere	Condition	MNI coordinate			Cluster size	Peak *t* value
			X	*Y*	*Z*		
Precuneus	Left	After < Before	− 7	− 56	48	73	5.014 1
Precentral gyrus	Left	After < Before	− 38	− 5	51		
Inferior frontal gyrus, orbital part	Left	After < Before	− 36	30	− 12	15	5.830 4
	Right		41	32	− 12		
Middle frontal gyrus, orbital part	Left	After < Before	30	50	− 9		
	Right		33	52	− 10		
Lingual gyrus	Left	After < Before	− 14	− 67	− 4	79	5.020 7
	Right		16	− 67	− 3		

voxel-by-voxel paired *t* test, it was found that after electroacupuncture stimulation, the DC values of the precuneus, orbitofrontal, anterior central, and lingual gyri decreased significantly; there was a significant difference after GRF correction (voxel $P < 0.001$, cluster $P < 0.05$).

4.2 ALFF analysis

The calculated results of ALFF by paired *t* test showed that after uterine-point acupuncture, the ALFF values of the cuneus, lingual gyrus, orbitofrontal cortex, and posterior cingulate cortex decreased, with a statistically significant difference after GRF correction (voxel $P < 0.001$ cluster $P < 0.05$). The experimental results and different areas are shown in Table 2 and Figure 4.

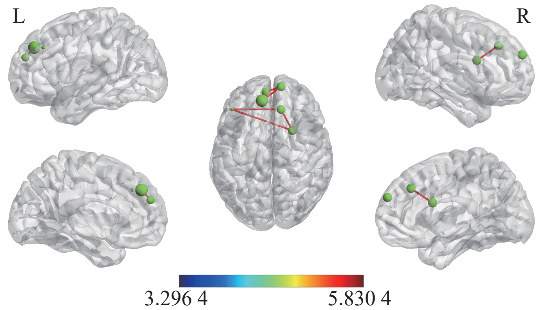

Figure 3 DC exhibited different brain regions after acupuncture intervention

L represents left; R represents right.

Table 2 Statistical analysis of ALFF difference brain area after acupuncture intervention

Brain region	Hemisphere	Condition	MNI coordinate			Cluster size	Peak *t* value
			X	*Y*	*Z*		
Precuneus	Left	Later < Before	− 7	− 56	48	141	4.442 2
Posterior cingulate gyrus	Left	Later < Before	− 5	− 43	24		
Superior frontal gyrus, orbital part	Left	Later < Before	− 16	47	− 13	122	4.502 6
	Right		18	48	− 14		
Lingual gyrus	Left	After < Before	− 14	− 67	− 4	79	5.020 7
	Right		16	− 67	− 3		

4.3 ReHo analysis

The data analysis of ReHo was similar to that of ALFF. The paired *t* test also conducted voxel-by-voxel based on the whole brain mask, with a statistically significant difference after GRF correction (voxel $P < 0.001$, cluster $P < 0.05$). Compared to the value prior to acupuncture intervention, the ReHo value decreased in the cuneus, lingual gyrus, orbitofrontal cortex, precentral gyrus, and amygdala after acupuncture (voxel $P < 0.001$, cluster $P < 0.05$). The results are presented in Table 3 and Figure 5.

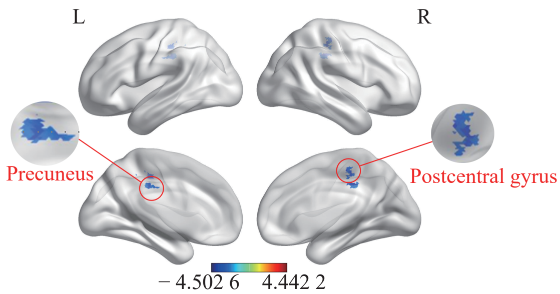

Figure 4 ALFF exhibited different brain regions after acupuncture intervention

L represents left; R represents right.

Table 3 Statistical analysis of ReHo difference brain area after acupuncture intervention

Brain region	Hemisphere	Condition	MNI coordinate			Cluster size	Peak *t* value
			X	*Y*	*Z*		
Precuneus	Left	After < Before	– 7	– 56	48	73	6.515 6
Precentral gyrus	Left	After < Before	– 38	– 5	51		
Superior frontal gyrus, orbital part	Left Right	After < Before	– 16 18	47 4	– 13 – 14	50	5.969 6
Lingual gyrus	Left Right	After < Before	– 14 16	– 67 – 67	– 4 – 3		
Amygdala	Left	After < Before	– 23	– 1	– 17	54	5.515 6

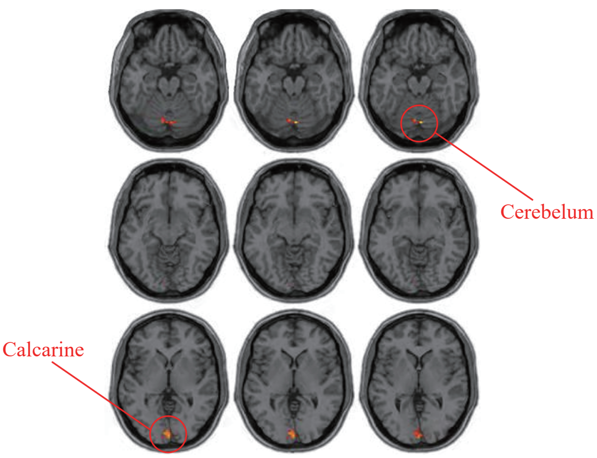

Figure 5 ReHo exhibited different brain regions after acupuncture intervention

4.4 ICA analysis

Infomax ICA was used to analyze functional connections after acupuncture intervention. Differential brain regions were identified using Infomax ICA; paired *t* test and GRF correction were performed on a voxel-by-voxel basis. Results demonstrated significant differences (voxel $P < 0.001$, cluster $P < 0.05$); it was found that uterine-point acupuncture enhanced the functional connection strength of the visual network and synergistically activated the hypothalamic-pituitary system (voxel $P < 0.001$, cluster $P < 0.05$). On the other hand, in the auditory network, the precuneus, cuneus, and lingual gyri and the hypothalamic-pituitary system were all inhibited. Furthermore, the overall functional connection strength of the right frontal-parietal network decreased (voxel $P < 0.001$, cluster $P < 0.05$), and the neural activity of the precuneus and calcarine sulcus was significantly weakened (voxel $P < 0.001$, cluster $P < 0.05$); however, the neural activities of the cerebellum and cuneus as well as the superior frontal, cingulate, and lingual gyri were enhanced (voxel $P < 0.001$, cluster $P < 0.05$).

A visual diagram of the effects of acupuncture on different brain networks is shown in Figure 6. Figures 6A, 6B, and 6C show schematic diagrams of the brain regions with differences in the auditory, visual, and right frontal-parietal networks of the brain before and after acupuncture. The blue region represents the weakening of the functional connection strength; the red region represents

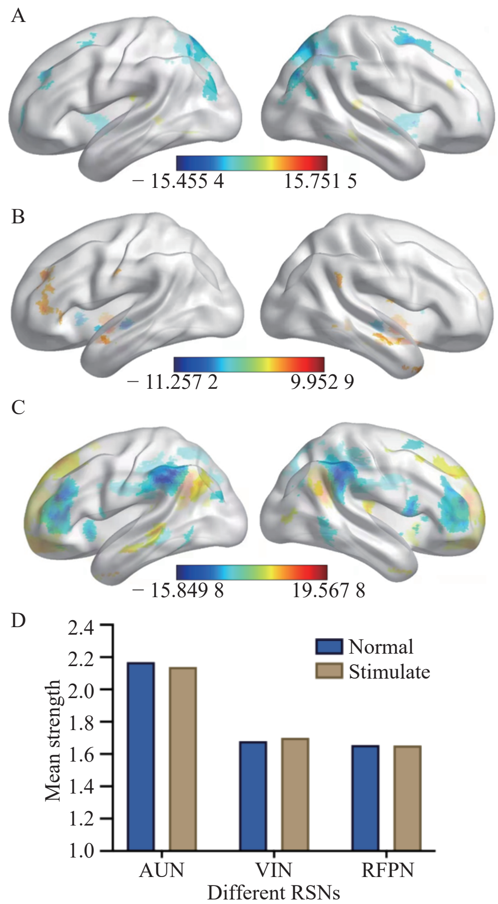

Figure 6 Visual schematic diagram of acupuncture effect of different brain networks

A, the difference of auditory network before and after acupuncture. B, the difference of visual network before and after acupuncture. C, the difference of right frontal-parietal network (AUN, VIN, RFPN, respectively) before and after acupuncture. D, the difference of average functional connection strength between auditory, visual and right frontal-parietal networks (AUN, VIN, and RFPN, respectively) before and after acupuncture.

the enhancement of the functional connection strength. Figure 6D shows the difference in the average functional connection strength between the auditory, visual, and right frontal-parietal networks before and after acupuncture. In the auditory and right frontal-parietal networks, the average functional connection strength after acupuncture decreased; in the visual network, the functional connection strength after acupuncture increased.

5 Discussion

With the continuous development of imaging techniques, fMRI techniques have been increasingly applied to investigate acupuncture, providing important tools and imaging support [11] for studying its mechanism of action in treating diseases [12]. However, few scholars have explored the mechanism of uterine-point acupuncture in treating gynecological diseases. By analyzing the brain image data of acupuncture at a specific uterine point, the mechanism of acupuncture at various uterine points is evaluated.

Analyses of local brain spontaneous activity applied in this study, such as DC, ALFF, and ReHo, are widely used to evaluate brain dysfunction and mechanistic research [13]; however, only one or two of these are typically considered in existing studies. LI et al. [14] explored the internal non-connection mode of the whole-brain functional network in patients with Parkinson's disease (mild cognitive impairment in PD, PD-MCI) who present with mild cognitive impairment; through DC, they concluded that PD-MCI was related to extensive regional brain dysfunction. Moreover, CUI et al. [15] used fractional amplitude of low-frequency fluctuation (fALFF) combined with DC to determine the presence of brain dysfunction in patients with somatic symptom disorders (SSD); this study was conducted to provide reference information for the clinical diagnosis and treatment of SSD. Another study by RESPINO et al. [16] used ReHo and network homogeneity to study the functional homogeneity of depression in later life; in this study, three analytical methods were used simultaneously. The different brain regions obtained by these methods were highly consistent; the results were more accurate and reliable.

Based on the analyses mentioned above and evaluation indices, it was found that acupuncture at various uterine acupoints reduced the neural activity intensity of the precuneus, orbitofrontal cortex, cerebellum, calcarine sulcus, lingual gyrus, amygdala, and postcentral gyrus. Based on previous studies [17-19], we speculated that acupuncture at bilateral uterine acupoints inhibited the neural activity intensity of the brain regions mentioned above, thus regulating the levels of female sex hormones, pain perception, and emotional changes to achieve physical and mental stability and for treating gynecological diseases.

As a data-driven analysis method, ICA does not need any prior knowledge, thereby avoiding the need to select a seed point or brain region as a prior hypothesis [20]. Infomax ICA transmits information upon maximization, tracks it to independent sources, and extracts the resultant information of brain functional connection before and after acupuncture at uterine acupoints [21]. Research on brain functional connectivity after uterine-point acupuncture demonstrated that this intervention could inhibit the functional connection between the auditory and the right frontal-parietal networks and activate the functional connection of the visual network.

The visual network includes the occipital and parietal regions [22]. We found that the precuneus and the postcentral, lingual, and middle occipital gyri were activated in the brain network. We also found that the hypothalamic-pituitary system was activated. We hypothesized that in the visual network, the hypothalamic-pituitary system, in coordination with the occipital and parietal lobes, regulates female hormone levels and mood changes, promotes female physical and mental pleasure, and maintains a good emotional state. In contrast, the postcentral gyrus plays an important role in treating dysmenorrhea. The auditory network is adjacent to the visual network, in which the precuneus and lingual gyrus and the hypothalamic-pituitary system are also inhibited; we speculated that these could be related to the regulation of anxiety and depression before and after the menstrual period. The right frontal-parietal network, which is involved in cognitive control and frontal eye movement, is concentrated in the angular gyrus, dorsolateral prefrontal cortex, and insula. This study indicated that after uterine-point acupuncture, the neural activity of the precuneus and calcarine sulcus decreased; the neural activity of the cerebellum, cuneus, and the superior frontal, cingulate, and lingual gyri increased; and the right frontal-parietal network was inhibited.

6 Conclusion

This study found that electroacupuncture at bilateral uterine acupoints can affect the neural activity intensity of the precuneus, orbitofrontal cortex, amygdala, precentral gyrus, postcentral gyrus, cerebellum, calcarine sulcus, and lingual gyrus. The brain regions mentioned above are consistent with the results of the differential brain network found by the ICA method; the ICA method further identifies the synergy between brain regions and the hypothalamic-pituitary system, thereby indicating that the method designed in this paper is consistent and accurate. Furthermore, this study has verified that after uterine-point acupuncture, the brain makes corresponding feedback, to which different brain regions cooperate with each other. Thus, this neural action is responsible for regulating women's cognition, sex hormone, and emotional levels relevant for disease treatment. This study aimed to investigate the mechanism of acupuncture at uterine acupoints and to provide imaging evidence for the mechanism of electroacupuncture at uterine acupoints. However, the etiology and pathogenesis of gynecological diseases are too complex. Therefore, to eliminate the interference of uncontrollable factors, this study analyzed the brain image data of healthy subjects to ensure the accuracy of the experimental results. Follow-up research can increase the number of subjects, introduce female samples with gynecological diseases, explore the mechanism of acupuncture at uterine acupoints in the treatment of gynecological diseases, and consider applying deep learning methods to better model brain function networks.

Fundings

National Nature Science Foundation of China (61872225), Natural Science Foundation of Shandong Province (ZR2020KF013, ZR2020ZD44, ZR2019ZD04, and ZR2020QF043), Introduction and Cultivation Program for Young Creative Talents in Colleges and Universities of Shandong Province (2019-173), and Special Fund of Qilu Health and Health Leading Talents Training Project.

Competing interests

The authors declare no conflict of interest.

References

[1] ZHANG Y, NONG ZN, ZHANG M. Ancient literature analysis of uterine acupoints in the treatment of gynecological diseases. Asia Pacific Traditional Medicine, 2014, 10(19): 56–57.

[2] SHEN XY, LIU CZ. Meridian Yu acupoints. The fifth edition. Beijing: Chinese traditional medicine press, 2021.

[3] LI J, HAO J, CHEN S, et al. Analysis of ancient literature on uterine acupoints for the treatment of gynecological diseases. Journal of Guangzhou University of Traditional Chinese Medicine, 2020, 37(4): 790–794.

[4] WANG Y, XU J, ZHANG Q, et al. Immediate analgesic effect of acupuncture in patients with primary dysmenorrhea: a fMRI study. Frontiers in Neuroscience, 2021, 15: 546.

[5] ZHU D, YUAN T, GAO J, et al. Correlation between cortical gene expression and resting-state functional network centrality in healthy young adults. Human Brain Mapping, 2021, 42(7): 2236–2249.

[6] ZANG Y, JIANG T, LU Y, et al. Regional homogeneity approach to fMRI data analysis. Neuroimage, 2004, 22(1): 394–400.

[7] ZANG YF, HE Y, ZHU CZ, et al. Altered baseline brain activity in children with ADHD revealed by resting-state functional MRI. Brain and Development, 2007, 29(2): 83–91.

[8] YAN CG, WANG XD, ZUO XN, et al. DPABI: data processing & analysis for (resting-state) brain imaging. Neuroinformatics, 2016, 14(3): 339–351.

[9] CALHOUN VD, POTLURU VK, PHLYPO R, et al. Independent component analysis for brain fMRI does indeed select for maximal independence. PloS One, 2013, 8(8): e73309.

[10] SMITH SM, FOX PT, MILLER KL, et al. Correspondence of the brain's functional architecture during activation and rest. Proceedings of the National Academy of Sciences, 2009, 106(31): 13040–13045.

[11] LIU CJ, CHEN ZH, LI SJ, et al. Visual analysis of research hotspots and frontiers on randomized controlled trials of acupuncture and moxibustion in the past 10 years. Chinese Acupuncture & Moxibustion: 1-12[2021-11-12]. doi: 10.13703/j.0255-2930.20201221-k0001.

[12] LI YC, CHEN YS, CHEN BJ, et al. BOLD-fMRI application value of BOLD-fMRI technique in the study of acupoint-brain effect. Journal of Clinical Acupuncture and Moxibustion, 2021, 37(7): 6–10.

[13] YUAN LX, ZHAO N, WANG XQ, et al. Echo time dependency of local activity metrics of resting-state functional MRI. Frontiers in Neuroscience, 2021, 15: 619412.

[14] LI MG, BIAN XB, ZHANG J, et al. Aberrant voxel-based degree centrality in Parkinson's disease patients with mild cognitive impairment. Neuroscience Letters, 2020, 741: 135507.

[15] CUI YY, LIANG HB, ZHU Q, et al. Resting state functional magnetic resonance imaging of somatic symptom disorder based on fALFF and DC. Chinese Journal of Magnetic Resonance Imaging, 2021, 12(7): 51–54.

[16] RESPINO M, HOPTMAN MJ, VICTORIA LW, et al. Cognitive control network homogeneity and executive functions in late-fife depression. Biological Psychiatry: Cognitive Neuroscience and Neuroimaging, 2020, 5(2): 213–221.

[17] LIU XR, ZANG ZW, LI XL, et al. Effectiveness of electroacupuncture of Zigong (EX-CA1), etc. in treatment of perimenopausal syndrome women. Acupuncture Research, 2016, 41(3): 247–250.

[18] YU YP, MA LX, MA YX, et al. Immediate effect of acupuncture at Sanyinjiao (SP6) and Xuanzhong (GB39) on uterine arterial blood flow in primary dysmenorrhea. The Journal of Alternative and Complementary Medicine, 2010, 16(10): 1073–1078.

[19] CHEN LM, LI XJ, XU K, et al. Functional MRI-based study on neuromchanism of trans-auricular vagus nerve stimulation for treatment-resistant depression. Acupuncture Research, 2021, 46(10): 869–874.

[20] LV H, WANG Z, TONG E, et al. Resting-state functional MRI: everything that nonexperts have always wanted to know. American Journal of Neuroradiology, 2018, 39(8): 1390–1399.

[21] DING SW. Brain network characterics in brain tumor patients revealed by functional network analysis based on fMRI dataset. Nanjing: Nanjing University of Aeronautics and Astronautics, 2014.

[22] KEANE BP, BARCH DM, MILL RD, et al. Brain network mechanisms of visual shape completion. NeuroImage, 2021, 236: 118069.

针刺子宫穴的静息态自发脑活动及功能连接分析

袁航[a, b], 于晓华[c], 李翔[a, b], 秦嗣钧[a, b], 梁桂香[a, b], 白田雨[d], 魏本征[a, b*]

a. 山东中医药大学青岛中医药科学院, 山东 青岛 266112, 中国
b. 山东中医药大学医学人工智能研究中心, 山东 青岛 266112, 中国
c. 山东中医药大学针灸推拿学院, 山东 济南 250355, 中国
d. 山东省立第三医院针灸推拿科, 山东 济南 250031, 中国

【摘要】目的 采用静息状态功能磁共振成像(rs-fMRI)分析方法,研究电针刺激双侧子宫穴(EX-CA1)引发的大脑活动及其功能连接情况,探究针刺子宫穴治疗妇科疾病的作用机制。**方法** 电针刺激 22 名健康女性受试者的双侧子宫穴,对受试者脑部 rs-MRI 数据做标准化预处理;采用度中心性、低频波动振幅和局部一致性方法,分析被试针刺前后的局部自发性脑活动;采用基于独立成分分析的功能连接分析方法,研究针刺前后静息态脑网络的连接情况。**结果** 局部自发性脑活动分析发现,与针刺前相比,针刺后受试者楔前叶、眶额皮层、舌回、杏仁核以及中央后回的神经活动强度降低 (体素 $P < 0.001$, 团簇 $P < 0.05$);功能连接分析发现,听觉网络和右侧额顶网络功能连接减弱 (体素 $P < 0.001$, 团簇 $P < 0.05$),视觉网络功能连接增强 (体素 $P < 0.001$, 团簇 $P < 0.05$),并且在听觉网络和视觉网络中发现下丘脑-垂体系统被协同激活。**结论** 研究结果表明针刺子宫穴前后,部分脑区的神经活动及功能连接存在明显差异,并且下丘脑-垂体系统的不同脑区也出现了不同的活跃状态。据此推测可知针刺子宫穴的作用机制与大脑调节生殖激素水平、情绪变化及躯体感觉有关。研究设计的脑影像分析方法,可在一定程度上阐明针刺子宫穴治疗妇科疾病的神经作用机制,并为针刺其他穴位的机制研究提供了可借鉴的分析方法。

【关键词】 子宫穴;针刺;功能磁共振成像;局部自发性脑活动分析;静息态;功能连接分析